Nonlinear elasticity in resonance experiments

Xun Li,[1,*] Christoph Sens-Schönfelder,[2] and Roel Snieder[1]
[1]*Center for Wave Phenomena, Colorado School of Mines, Golden, Colorado 80401, USA*
[2]*GFZ German Research Centre for Geosciences, Potsdam, Germany*

(Received 8 January 2018; revised manuscript received 19 January 2018; published 16 April 2018)

Resonant bar experiments have revealed that dynamic deformation induces nonlinearity in rocks. These experiments produce resonance curves that represent the response amplitude as a function of the driving frequency. We propose a model to reproduce the resonance curves with observed features that include (a) the log-time recovery of the resonant frequency after the deformation ends (slow dynamics), (b) the asymmetry in the direction of the driving frequency, (c) the difference between resonance curves with the driving frequency that is swept upward and downward, and (d) the presence of a "cliff" segment to the left of the resonant peak under the condition of strong nonlinearity. The model is based on a feedback cycle where the effect of softening (nonlinearity) feeds back to the deformation. This model provides a unified interpretation of both the nonlinearity and slow dynamics in resonance experiments. We further show that the asymmetry of the resonance curve is caused by the softening, which is documented by the decrease of the resonant frequency during the deformation; the cliff segment of the resonance curve is linked to a bifurcation that involves a steep change of the response amplitude when the driving frequency is changed. With weak nonlinearity, the difference between the upward- and downward-sweeping curves depends on slow dynamics; a sufficiently slow frequency sweep eliminates this up-down difference. With strong nonlinearity, the up-down difference results from both the slow dynamics and bifurcation; however, the presence of the bifurcation maintains the respective part of the up-down difference, regardless of the sweep rate.

DOI: 10.1103/PhysRevB.97.144301

I. INTRODUCTION

Resonant bar experiments can be used to measure the nonlinear elasticity of natural rocks or concrete and further monitor small changes of elasticity (velocity) with high accuracy [1–3]. In resonance experiments, a dynamic normal force imposes cyclic compressions and extensions on a cylindrical rod with a driving frequency that can be changed, continuously sweeping towards higher or lower values [4–6]. For each driving frequency, the dynamic deformation of the rod gradually reaches a state where the oscillation has a stable amplitude; such an amplitude defines the measured response for the corresponding driving frequency [6–8]. The dependence of the response amplitude on the driving frequency generates a resonance curve that can be used to characterize the elastic property of rocks [1].

Laboratory measurements produce resonance curves with the following features [1–3,6–8]. The resonant peak shifts towards lower frequency for an increasing driving force and shifts back towards higher frequency in the recovery process [9]. The resonant frequency recovers with the logarithm of time after the deformation ends (slow dynamics) [2]. Resonance curves are asymmetric along the frequency axis around their peak frequency as soon as the driving force is strong enough to induce softening [3]. With an increase in the driving force, the resonance curve steepens to the left of the resonant peak and flattens to the right of the peak. TenCate and Shankland [1] show that a difference exists between the upward and downward resonance curves, produced by sweeping the driving frequency upward and downward, respectively. This up-down difference is most pronounced to the left of the resonance. TenCate [3] finds that a slow sweep of the driving frequency can eliminate the up-down difference and produce the same resonance curves, regardless of the sweep direction. Johnson *et al.* [7] show that strong nonlinearity in rocks induces a vertical segment of the resonance curve to the left of the resonant peak. This vertical segment, which we refer to as the "cliff," involves a large abrupt change of the response amplitude when the driving frequency is increased/decreased. The response amplitude changes upward/downward along the cliff as the driving frequency passes the resonant peak. We present a theory for the above-mentioned experimental features of resonance curves using a simple thermodynamics-based model.

In this paper, Sec. II starts from a feedback cycle as the framework of our thermodynamics-based model; we then propose the relationship between dynamic deformation and thermal activations/relaxations of fractures. Taking the feedback of the fracture behavior on Young's modulus into account, we conduct the simulation of resonance experiments following the protocol used in the laboratory (Sec. III). Section IV shows that our model can reproduce resonance curves with the observed features, including (a) the slow dynamics with log-time recovery, (b) the asymmetry of resonance curves, (c) the disappearance of the up-down difference at a slow sweep rate of the driving frequency, and (d) the presence of the cliff in the resonance curve when the nonlinearity is strong. Additionally, our model predicts that the steep cliff with strong nonlinearity is related to a permanent up-down difference that does not vanish for a slow sweep rate. This has not been observed experimentally, yet. Finally, in Sec. V, we propose a unified interpretation of all these observed features; this

*Corresponding author: lixun@mines.edu

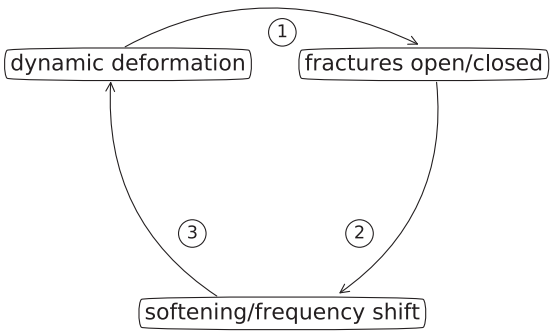

FIG. 1. Feedback cycle for nonlinear material properties.

interpretation enhances the understanding of both the nonlinear elasticity and slow dynamics in resonance experiments.

II. MODEL

Different micromodels can simulate resonance experiments where dynamic deformation leads to a reduction of resonant frequency (Young's modulus); this reduction reflects the softening of rocks [7,10–13]. We propose a simple thermodynamics-based model, following Refs. [14–17] that is based on (a) bond rupture/healing and (b) an oscillation equation, to simulate both slow dynamics and resonance curves. Our model can include the concept of "effective" granular temperature for the vibration energy [18–20]. However, our model does not involve a detailed upscaling generalization from microscale to macroscale and does not rely on a complex description of physics mechanisms as in earlier work [9,21,22].

A. Feedback cycle

We use a feedback cycle for the material response shown in Fig. 1 that is akin to a theory for liquefaction [23]. The feedback cycle is the base of the thermodynamics-based parametrization in our model. Link 1 in the cycle accounts for the change of fracture system due to dynamic deformation, while link 2 describes the change in the elasticity (softening) due to the opening of fractures. The change of the elasticity feeds back to the deformation amplitude (link 3). We use "fractures" as a general term for cracks, contacts, bonds, and microcontacts. A solid sample contains fractures with scales ranging from microscopic dislocation defects in crystals to mesoscopic granular contacts and to macroscopically visible cracks.

B. Thermodynamics-based parametrization

We consider a bistable model where a fracture can be in one of two configurations: open or closed, with associated energy levels E_o and E_c, respectively, as shown in Fig. 2. We assume that an energy barrier E_b needs to be overcome for the fracture to change the configuration. This bistable model follows earlier energy models for the fracture contact [9,15,21,24].

We further consider that due to the thermal energy k_BT, a fracture can spontaneously change its configuration with characteristic transition times τ_o to close a fracture and τ_c to open a fracture, following Arrhenius' law [25,26]:

$$\tau_o = Ae^{(E_b-E_o)/k_BT}, \quad \tau_c = Ae^{(E_b-E_c)/k_BT}. \tag{1}$$

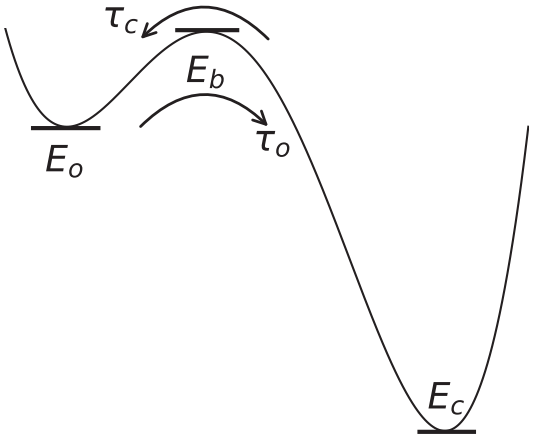

FIG. 2. Bistable energy model for a fracture. For a barrier energy E_b, τ_c and τ_o indicate the transition times to open and close the fracture, respectively.

E_o and E_c are the energies of open and closed fractures, respectively. E_b is the barrier energy, k_B is the Boltzmann constant, T is the temperature, and A is a time constant. The bistable dynamic equation for a group of fractures with the same barrier energy is

$$\frac{dn_o}{dt} = -\frac{n_o}{\tau_o} + \frac{1-n_o}{\tau_c}, \tag{2}$$

where n_o is the fraction of open fractures for a given barrier energy, and $n_c = 1 - n_o$ is the fraction of closed fractures. In Eq. (2), the first term on the right-hand side indicates the rate at which fractures close while the second term indicates the rate at which fractures open. In equilibrium $dn_o/dt = 0$, and thus the corresponding fraction $n_{\rm eq}$ of open fractures is

$$n_{\rm eq} = \frac{1}{1+\exp[(E_o-E_c)/k_BT]}, \tag{3}$$

and hence $n_{\rm eq}$ is independent of the barrier energy. For $E_o \gg E_c$, most fractures are closed while with $E_c \gg E_o$, most fractures are open.

We assume that the barrier energies that correspond to fractures with different sizes are distributed uniformly in an interval $[E_{b\,\min}, E_{b\,\max}]$. The aggregate fracture system that includes fractures with different barrier energies has an average fraction of open fractures $N_o(t) = \int_{E_{b\,\min}}^{E_{b\,\max}} n_o(E_b,t)dE_b/(E_{b\,\max} - E_{b\,\min})$.

The fracture system affects the elasticity of the material [27,28]; the opening of fractures lowers Young's modulus. For the link 2 in Fig. 1, we linearize the relationship between Young's modulus Y and the fracture system N_o using

$$Y = Y_0 - C_0(N_o - N_{\rm ori}). \tag{4}$$

$N_{\rm ori}$ is the equilibrium fraction of open fractures with zero strain ($\epsilon = 0$), C_0 is the fracture modulus, and Y_0 is the static Young's modulus of the unperturbed sample. Link 3 in Fig. 1 indicates the feedback of the softening (reduction of Young's modulus) on the deformation amplitude; the feedback is introduced as a dependence of the energies E_c and E_o on the externally applied stain.

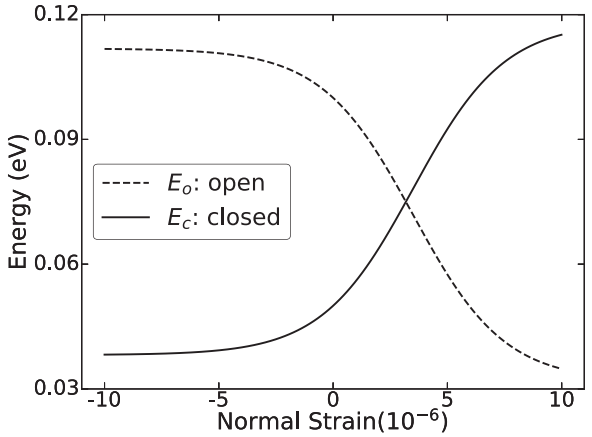

FIG. 3. Energy levels of open and closed fractures as a function of the dynamic normal strain. Positive strain corresponds to extension and negative strain corresponds to compression.

We propose a dependency of the energies of open and closed fractures as shown in Fig. 3; this dependency is parameterized by the sigmoid functions:

$$E_o(\epsilon) = B_0 - \frac{A_1}{1 + \exp[-(\epsilon - \mu)/\sigma]} \tag{5}$$

and

$$E_c(\epsilon) = A_0 + \frac{A_1}{1 + \exp[-(\epsilon - \mu)/\sigma]}, \tag{6}$$

where A_0, A_1, B_0, μ, and σ are constants, and ϵ is dynamic strain. This relationship is based on the premise that the deformation strain is the main factor affecting the nonlinear elasticity of rocks [29]. The nonlinearity of rocks becomes significant when the strain is of the order of a microstrain (10^{-6}) [10,29,30]. Thus, we prescribe a fracture energy that changes significantly once the strain is above 10^{-6}. For the strain range shown in Fig. 3, the fracture energy implies (a) that extension opens fractures (softening) while compression closes fractures (hardening), and (b) that the response to deformation is not symmetric for the positive and negative strain. The asymmetry reflects that the elastic response is more sensitive to extension (positive strain) than to compression (negative strain) [31,32]. However, the choice of the sigmoid function is quite arbitrary; it provides a smooth transition from a region that favors closed fractures to a region that favors open fractures. Figure 3 and the bistable model in Fig. 2 act as the link 1 in Fig. 1. We summarize the parameters used and their numerical values in Table I.

For a temperature $T = 300$ K, the thermal energy is $k_B T = 0.026$ eV. The energy difference between open and closed fracture in Fig. 3, together with Eq. (3), implies that for large positive strain ($\varepsilon \gtrsim 7 \times 10^{-6}$) the system favors open fractures, while for compression and small positive strain ($\varepsilon \lesssim 10^{-6}$) the system favors closed fractures. This description of fracture behavior is not necessarily accurate in its details and so should be seen as a plausible parametrization of fracture behavior. For some aspects of nonlinear material properties, the model may need to be extended to include the strain rate $\dot{\varepsilon}$ as well as shear deformation [33,34].

TABLE I. Numerical values of the parameters used.

	Definition	value
A	Time constant	1.0 s
T	Temperature	300.0 K
$E_{b\,\mathrm{min}}$	Minimum barrier energy	0.223 eV
$E_{b\,\mathrm{max}}$	Maximum barrier energy	0.401 eV
A_0	Constant	0.038 eV
A_1	Constant	0.080 eV
B_0	Constant	0.112 eV
μ	Constant	3.5×10^{-6}
σ	Constant	2.0×10^{-6}
L_0	Length of sample	0.3 m
ρ	Density of sample	2200 kg/m^3
Y_0	Static Young's modulus	12.05 GPa
C_0	Fracture modulus	1.853 GPa
f_0	Static resonant frequency	3900 Hz
γ	Damping factor	90.0 rad/s
t_0	Numerical time step	5 μs
τ_{max}	Maximum relaxation time	500 ms
Δt	Sweep time interval	5 ms
Δf	Sweep frequency interval	1 Hz

III. RESONANCE SIMULATION

We describe the deformation in the resonant bar experiment by

$$\frac{\partial^2 R_A}{\partial t^2} + 2\gamma \frac{\partial R_A}{\partial t} + \Omega^2 R_A = A_r e^{-i\omega t}, \tag{7}$$

where R_A is the dimensionless strain amplitude [i.e., ϵ in Eqs. (5) and (6)] in response to the driving field $A_r \sin(\omega t)$, γ is the damping factor, ω is the driving angular frequency, and Ω is the resonant angular frequency. The driving amplitude A_r is related to the driving force F_r using $A_r = F_r/ML_0$, where M is the mass and L_0 is the length of the sample. In Eq. (7), the resonant angular frequency incorporates the softening because it depends on Young's modulus $\Omega = \pi\sqrt{Y/\rho}/L_0$, where ρ is density [7]. To first order, the resonant angular frequency shift relates to the reduction of Young's modulus by $\Delta\Omega/\Omega_0 = \Delta Y/2Y_0$, where Ω_0 corresponds to the static Young's modulus Y_0 since $\Delta\Omega$ and ΔY are small compared to Ω_0 and Y_0. Solving Eq. (7) for a solution $R_A e^{-i\omega t}$ yields for the absolute value of the response

$$|R_A| = \frac{|A_r|}{\sqrt{(\omega^2 - \Omega^2)^2 + 4\gamma^2\omega^2}}. \tag{8}$$

We numerically simulate the measurement protocol (see Appendix A) used in the experiments (e.g., [6,7]). The recorded quantity for the response is the acceleration amplitude $\omega^2 R_A L_0$.

IV. NUMERICAL SIMULATIONS

We show in this section with our thermodynamics-based model that we can simulate important features (mentioned in Sec. I) of resonance curves produced in the laboratory [1–3,7].

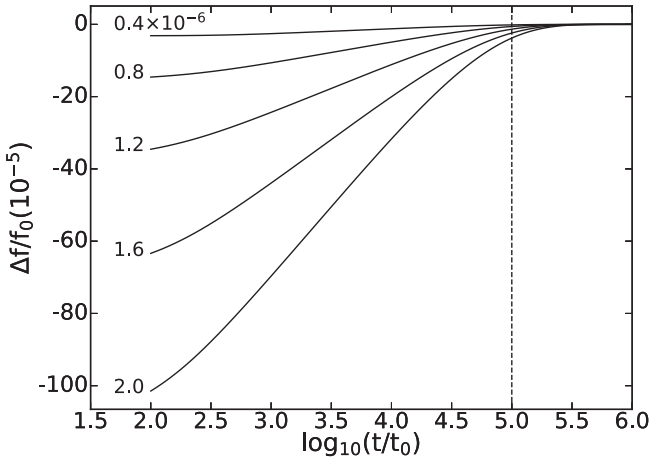

FIG. 4. Recovery of the resonant frequency after dynamic deformations with different strain amplitudes, where $t_0 = 5\ \mu$s is time step in the numerical model. The vertical dashed line denotes τ_{max}.

A. Recovery of resonant frequency

We simulate slow dynamics after the dynamic deformation ends. Figure 4 shows the recovery of the resonant frequency after long-time deformation (10^6 time steps or 5 ms) as a function of the logarithm of time. We use different amplitudes at the same driving frequency 3900 Hz. The log-time recovery produced by our model is (almost) identical to the laboratory measurements in Fig. 5 of TenCate *et al.* [2] that show the observed logarithmic recovery of the resonant frequency.

To illustrate the effect of the superimposed time scales, we can also apply the model without integrating over the barrier energy and show an example for a single barrier energy, $E_b = 0.38$ eV, in Fig. 5. In this case, the recovery does not vary with the logarithm of time. This highlights the importance of the summation of multiscale relaxation processes for the log-time recovery. Snieder *et al.* [35] propose τ_{max}, a metric to characterize the maximum relaxation time among multiscale

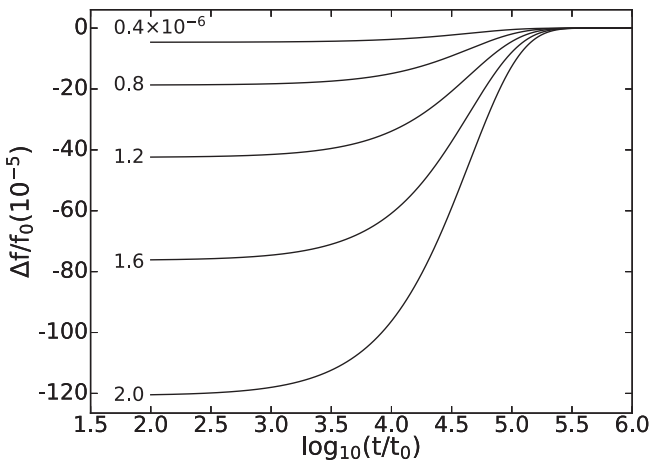

FIG. 5. Recovery of the resonant frequency for a single barrier energy.

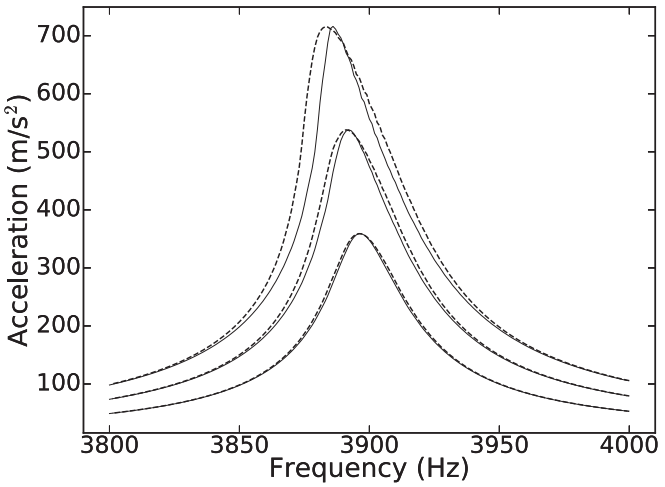

FIG. 6. Resonance curves for the upward (solid lines) and downward (dashed lines) sweeps with different driving amplitudes $A_r = 8.8, 13.2, 17.6/s^2$.

relaxation processes:

$$\frac{1}{\tau_{max}} = \left(\frac{1}{\tau_o} + \frac{1}{\tau_c}\right)_{E_b = E_{b\,max}}, \tag{9}$$

where τ_o and τ_c are given in Eq. (1). We denote τ_{max} in Fig. 4 with a dashed line, which agrees well with the time needed for the relaxation.

B. Asymmetric resonance curves

We show the response amplitude against the driving frequency in Fig. 6 for both the upward and downward sweeps and different driving amplitudes. We record the response as the acceleration given by $\omega^2 R_A L_0$ and change the driving frequency by $\Delta f = 1$ Hz after a time interval $\Delta t = 5$ ms ($0.01\tau_{max}$); the frequency sweep covers the resonant frequency $f_0 = 3900$ Hz of the unperturbed sample. Here we define Δt as the sweep time interval, which reflects the sweep rate of the driving frequency. One can regard Δt as the time duration between two consecutive driving frequencies. The total sweep time of the driving frequency results from the multiplication of Δt and the number of sampled driving frequencies.

Figure 6 shows that with increasing driving amplitude A_r, the peak value of the resonance curve increases and the resonant frequency decreases. An increase in the driving amplitude A_r gives an increase in the response amplitude [see Eq. (8)] and creates more open fractures than a low driving amplitude; the associated softening reduces the resonant frequency. The difference between the upward and downward resonance curves is reproduced by the model in all details and is most pronounced to the left of the resonant peak. Figure 6 can be qualitatively compared to the laboratory measurements in TenCate and Shankland [1], especially for the asymmetric resonance curves when the driving amplitude is large.

The asymmetry in the direction of the driving frequency can be explained as follows. Suppose one sweeps downward in frequency. When the frequency is higher than the resonant frequency ($\omega > \Omega$) and one approaches the resonant peak, the deformation increases and the sample softens. This reduces

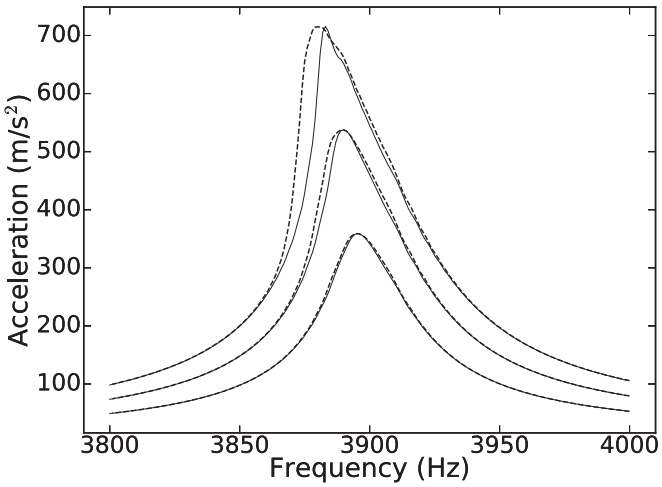

FIG. 7. Resonance curves as in Fig. 6, but for a single barrier energy.

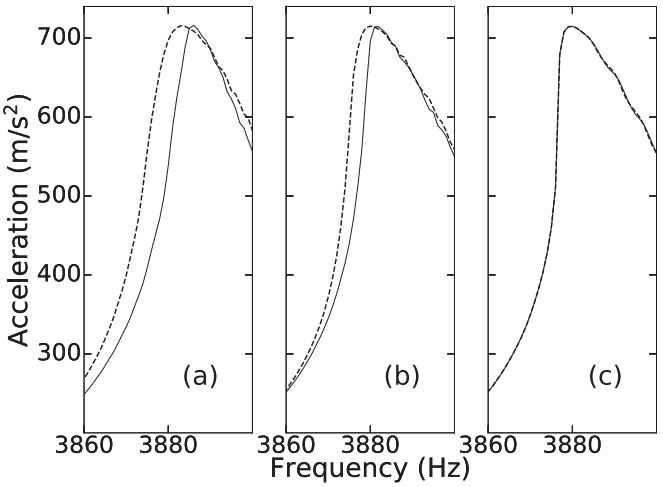

FIG. 8. Sweep-rate dependence of the up-down difference of the resonance curves at the left side of the resonant peak. Solid lines denote the upward sweep, while dashed lines denote the downward sweep. The sweep time interval between sampled driving frequencies is (a) 5 ms ($0.01\tau_{\max}$), (b) 500 ms ($\tau_{\max}$), and (c) 5 s ($10\tau_{\max}$).

the resonant frequency Ω, hence the resonant peak "moves away" from the current driving frequency ω, and as a result the response curve flattens to the right of the peak. But when the driving frequency is reduced further, the driving frequency ω is less than the resonant frequency Ω. Now the deformation decreases as the driving frequency is reduced further, which makes the sample stiffer. This increases the resonant frequency Ω, which moves the response peak towards higher frequency, away from the current frequency, which further decreases the deformation. Thus, this increasing resonant frequency leads to a steepening of the resonance curve to the left of the peak. A similar reasoning applies when one increases the driving frequency ω starting at values less than the resonant frequency Ω. Approaching the resonant peak from the left, the peak of the curve comes closer when the amplitude increases; consequently, it steepens on the left and it flattens on the right. The asymmetry of the resonance curve thus follows from the nonlinearity that causes the sample to soften as the deformation increases. In our model, the nonlinearity is implicit in the used parametrization of the fracture behavior and its imprint on Young's modulus, but a nonlinear model based on anharmonicities gives the same shape of resonance curves [13]. In other words, softening (nonlinearity) steepens the left part of the resonance curve and flattens the right part, which is equivalent to the mechanism that the feedback of the nonlinearity on deformation causes the shift of the resonant frequency.

We can apply the model without integrating over the barrier energy and show an example for a single barrier energy $E_b = 0.30$ eV. Figure 7 shows the resonance curves for this case. The resonance curves in Fig. 7 have (almost) the same shapes as those in Fig. 6. We have shown that the multiscale relaxation mechanism is essential to the log-time recovery in Sec. IV A. However, comparing Figs. 6 and 7, we conclude that the multiscale relaxation mechanism is not essential for the shape of resonance curves.

C. Up-down difference and slow dynamics

TenCate and Shankland [1] speculate that for a slow sweep rate, i.e., large Δt of the driving frequency, the up-down difference disappears. For a slow sweep rate, the activation is effectively stationary in time, and one would expect that the sample reaches an equilibrium that is the same, regardless of whether one sweeps up or down. TenCate [3] confirms the speculation that the up-down difference can vanish at a slow sweep rate in the laboratory measurements.

Figure 8 shows the up-down difference at different sweep rates with a driving amplitude $A_r = 17.6/\text{s}^2$ corresponding to the uppermost pairs of the resonance curves in Fig. 6. The simulation in this figure confirms the speculation in [1] and echoes the laboratory measurements [3] in which a slow sweep rate eliminates the up-down difference [see Fig. 8(c)]. We compare the sweep rate (sweep time interval Δt) to the maximum relaxation time $\tau_{\max}$ in our model. For the used sweep frequency interval $\Delta f = 1$ Hz, we refer the fast sweep to the case $\Delta t \ll \tau_{\max}$ while the slow sweep means $\Delta t \gg \tau_{\max}$. We attribute the up-down difference to slow dynamics when the sweep is fast [e.g., Fig. 8(a)]. That a driving frequency gives different response amplitudes for different sweep directions reflects that the fracture system memorizes the past deformation (slow dynamics). However, as the sweep rate decreases, this "memory effect" disappears and the driving force conditions the sample to the same response amplitude regardless of the sweep direction.

D. Cliff in resonance curves

We further increase the nonlinearity in the simulation by increasing the value of the fracture modulus C_0. Figure 9 shows the dependence of the up-down difference on the sweep rate. Comparison of Figs. 8 and 9 indicates that nonlinearity enhances the up-down difference. Strong nonlinearity and a slow sweep rate can produce a "cliff" (vertical segment) in resonance curves [e.g., Fig. 9(c)]. The cliff represents a large abrupt change of the response amplitude when the driving frequency is changed. The up-down difference right at the cliff does not disappear for slow sweep rates, even though it vanishes away from the cliff [Fig. 9(c)]. This appears very

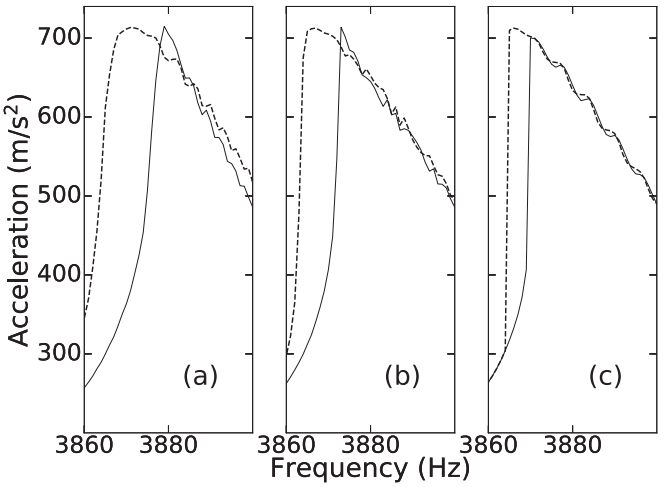

FIG. 9. Sweep-rate dependence of the up-down difference. The fracture modulus is $C_0 = 3.088$ GPa, with stronger nonlinearity than that in Fig. 8. The sweep time interval between sampled driving frequencies is (a) 5 ms ($0.01\tau_{\max}$), (b) 500 ms ($\tau_{\max}$), and (c) 5 *s* ($10\tau_{\max}$), following Fig. 8.

similar to the measurements by Johnson *et al.* [7], who show resonance measurements in Lavoux sandstone that exhibit a cliff with a pronounced difference between upward and downward sweeps.

To explain the up-down difference that is most pronounced in Fig. 9(c) at the cliff even when the sweep rate is slow, we refer to the bifurcation that originates from the solution of the Duffing equation for nonlinear systems [36–38]. We consider the steady-state solution of our model without incorporating the temporal evolution of the fracture system, i.e., the fraction of open fractures N_o in stable equilibrium where N_o represents the damage of the sample. We then solve for the damage N_o from different initial damage N_{oi} at each fixed frequency (for more details, see Appendix B). Figures 10(a) and 10(b) show the stable equilibrium damage state for every frequency (i.e., dashed black and solid green curves) for two different driving amplitudes; the colors indicate that for each frequency and initial value N_{oi} the final fraction of open fractures N_o to which the system converges (see Appendix B). Figure 10(a) shows the situation for moderate nonlinearity caused by a driving amplitude of $0.6/\text{s}^2$. In this case the stable equilibrium damage state N_o is determined only by frequency. Independently of the initial damage state, the system converges to the same stable equilibrium indicated by the overlapping lines. The situation is different for stronger nonlinearity, as shown in Fig. 10(b), where there is a range of frequencies in which the stable equilibrium damage state to which the system converges also depends on the initial damage state. Figure 10(b) shows a bifurcation of the stable equilibrium solution N_o; for a range of driving frequencies around the cliff of the resonance curve, there are two possible solutions of N_o for the same driving frequency. When one *reduces* the driving frequency ω at point d in Fig. 10(b), the system can only jump to point a. This leads to the vertical slope of the dashed line in Fig. 9(c). A similar reasoning applies to sweeping upward in frequency. When sweeping upward, one arrives at point b of the resonance curve. When sweeping further upward in frequency, the system jumps to point c on the resonance curve, and this jump results in a vertical segment of the resonance curve at a higher frequency.

The steady-state solution can be indicative of the simulated resonance experiment. We argued above that the nonlinear material response causes the response curve to steepen to the left of the resonant peak. The feedback of the deformation on the response can be so strong that the resonance curve folds over on itself, as shown in Fig. 10(b); this folding happens when the nonlinearity caused by a large driving force is sufficiently strong. When the nonlinearity is further increased, a bifurcation occurs [Fig. 10(b)]. Thus, this phenomenon of vertical jumps in the resonance curves corresponds to a bifurcation caused by the nonlinearity in the underlying equations with time evolution. A prototype of this bifurcation is described for the Duffing equation [36], which can be solved using the harmonic balance method [37]. The stable equilibrium solution is a simplified solution corresponding to the approximation that one can omit the details of the averaged fracture system during an oscillation cycle. Note that along segment $\overline{db}$ in Fig. 10(b), there is an abrupt change in color. For initial values just above the segment the damage will increase

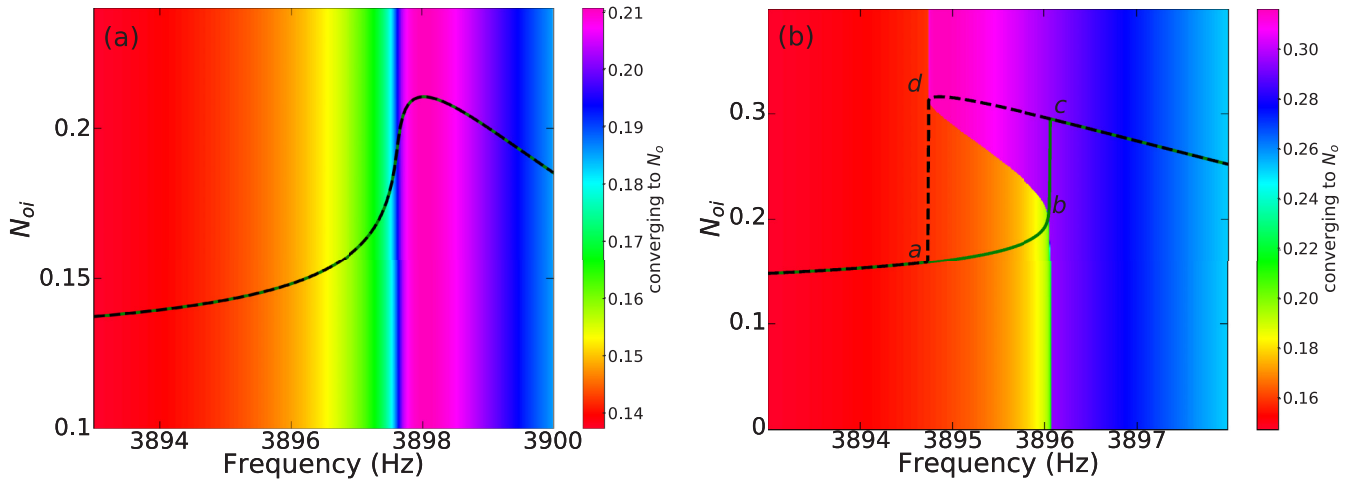

FIG. 10. Steady-state solution of our model with (a) $A_r = 0.6/\text{s}^2$ and (b) $A_r = 1.0/\text{s}^2$. The color scale indicates for each frequency and original value N_{oi} the equilibrium fraction N_o to which the solution converges.

and the system converges to a higher equilibrium value along segment $\overline{cd}$, while for initial values below segment $\overline{db}$ the system relaxes to a lower equilibrium value along segment $\overline{ab}$. This means that just as with the Duffing equation [36], segment $\overline{db}$ corresponds to unstable equilibrium values.

The stable equilibrium solution further indicates that the key factor for the system to lock in to a solution depends on the current value of N_o when the driving frequency is changed. Changing the sweep direction results in a different initial damage with which a certain frequency is approached, and in the case of strong nonlinearity, a different sweep direction might lead to a different stable equilibrium to which the system converges. However, the bifurcation is only present when the nonlinearity is sufficiently strong to cause a vertical cliff. The nonlinearity (bifurcation) can originate from both (a) large driving amplitudes and (b) material properties (e.g., the opening and closing of fractures with strain, and the influence of fractures on the modulus).

Since different nonlinear models to lowest order reduce to a cubic term (Duffing equation) in the equation of motion, this catastrophic behavior (vertical cliff with strong response to tiny change in frequency) is displayed by different models for nonlinear rock physics [7,13,39]. However, these models do not explicitly explain the cliff in the resonance curve by the bifurcation. In contrast to earlier work [14,17], our model is significantly simpler and is based on a relation between the (micro)fracture energy and strain; this relation is another form of thermodynamics-based parametrization. Vakhnenko *et al.* [14] relate the up-down difference to the end-point memory (slow dynamics) but do not show this catastrophic behavior (cliff) in resonance curves. Regarding slow dynamics, Fig. 4 gives a better straight-line region than Fig. 11 in Vakhnenko *et al.* [14]. Lyakhovsky *et al.* [17] show the cliff in the simulated resonance curve but do not relate the cliff with the bifurcation. Our theory qualitatively reproduces both the slow dynamics and bifurcation observed in laboratory experiments [1,7].

V. DISCUSSION

The resonance curves in Fig. 6 show two conspicuous features: they are asymmetric, and they are different depending on whether one sweeps upward or downward in frequency (up-down difference). We explain the asymmetry of resonance curves by softening (nonlinearity) and the up-down difference by both the slow dynamics and bifurcation. It is the nonlinearity that produces the bifurcation. The bifurcation occurs only when the nonlinearity is sufficiently strong. The bifurcation causes a cliff in resonance curves [37]; otherwise, in the absence of a bifurcation (for weaker nonlinearity) slow dynamics dominates the up-down difference, and this difference disappears for slow sweep rates. The reports of the coincidence of the resonance curves, e.g., [1,3], are for cases where slow dynamics dominates the up-down difference. The nonlinearity of rocks in these experiments [1,3] is not strong enough to cause a bifurcation. Johnson *et al.* [7] show the experimental resonance curves with cliff segments that result from the strong nonlinearity in rocks. Our model also reproduces this cliff behavior (Fig. 9) when the nonlinearity is significantly strong. Even stronger nonlinearity causes the system to display chaotic behavior [40] where the response amplitude jumps up and down.

In summary, up-down resonance curves can be coincident at a slow sweep rate, but only if the nonlinearity is weak. When the cliff is observed in resonance curves, our model predicts that no matter how slowly one sweeps the driving frequency, the up-down resonance curves cannot be coincident because of the presence of a bifurcation. Figure 9 confirms our conclusion that the up-down difference for slow sweep rates does not vanish when the system is bifurcated.

Slow dynamics is caused by the nonlinear rock properties. Such nonlinearity can be caused by (a) classical anharmonicity from Landau's theory [31] or (b) nonclassical anharmonicity from Hertz-Mindlin contacts [9]. In addition, slow dynamics depends on a dependence of the nonlinearity on past deformation. When the sweep rate is not slow compared to the minimum relaxation time [Fig. 9(a)], the current response depends on the past deformation. This effectively smears out the cliff in the resonance curve.

VI. CONCLUSION

A simple thermodynamics-based model can explain observed resonance curves. But this model does not provide a unique description of the microscopic behavior of fractures as in studies for a physical origin of rate and state friction [41,42]. The theory can be treated as a phenomenological parametrization of the imprint of damage on crack properties. We prescribe the fracture energy in Fig. 3 in a heuristic fashion for compressive waves. In real rocks, shear motion occurs near fractures, even when the sample is under a compressive uniaxial load. In addition, the fracture behavior likely depends on the strain rate $\dot{\varepsilon}$ as well [33,34]. Fractures have a range of orientations with respect to the principal stress components, and the fracture behavior depends on a range of physical and chemical processes that are influenced by the presence of fluids (notably, water). Our model should be seen as a thermodynamics-based parametrization of nonlinear fracture behavior. But this simplified model can reproduce the experimental features of the observed resonance curves.

Our model offers a unified interpretation of both the nonlinearity and slow dynamics in resonance experiments. When the nonlinearity of the vibration system is weak, the up-down difference is indicative of slow dynamics. Thus, the up-down difference can be used to study the slow dynamics. When the nonlinearity is strong, the up-down difference depends on both the bifurcation and slow dynamics. In this case the up-down difference does not vanish around the cliff, no matter how slowly one sweeps the driving frequency in the resonance experiments. We suggest that one test the presence of the bifurcation in an experiment that is performed at a constant frequency within the relevant frequency range. When starting with a fully relaxed sample, the resulting stable equilibrium will be on the lower branch of the bifurcation. When starting with a sample that has been damaged by a sustained large driving amplitude, the sample will reach a stable equilibrium at the upper branch of the bifurcation.

ACKNOWLEDGMENT

We thank anonymous reviewers for their positive and constructive comments. This work was supported by the

Consortium Project on Seismic Inverse Methods for Complex Structures at the Colorado School of Mines.

APPENDIX A: MEASUREMENT PROTOCOL

We numerically simulate the measurement protocol used in the laboratory experiments, e.g., [6,7]:

(1) At a time $t = t_1$, we apply a dynamic force field to the sample with driving frequency $f_d = \omega/2\pi$ and driving amplitude A_r that is kept fixed. We calculate the oscillation (response) strain amplitude $R_A(t_1)$ using Eq. (8), where the softening of the material ($\Delta\Omega/\Omega = \Delta Y/2Y$) at $t = t_1$ is taken into account.

(2) For a duration $\Delta t = 5$ ms ($0.01\tau_{\max}$) the driving frequency is kept fixed, as the sample oscillates with the dynamic strain $\epsilon(t) = R_A(t)\sin[\omega(t - t_1)]$ until the time $t = t_1 + \Delta t$. Following the fracture energy in Fig. 3, we convert the dynamic strain ϵ to energy variations $E_o(t)$ and $E_c(t)$. Equation (1) then provides time-dependent transition times $\tau_o(t)$ and $\tau_c(t)$, which we use to integrate the right-hand side in Eq. (2) and solve the fraction of open fractures $n_o(E_b,t)$ for a given barrier energy E_b. We average $n_o(E_b,t)$ over the barrier energy interval $[E_{b\min}, E_{b\max}]$ and obtain the temporal variation of $N_o(t)$ during the oscillation. N_o is the fraction of open fractures in the sample averaged over barrier energies. $N_o(t)$ leads to the softening $\Delta Y = Y - Y_0$ through Eq. (4). We average $N_o(t)$ over the past cycle of strain oscillation (with time duration $1/f_d$); from this averaged value, we calculate the dynamic Young's modulus Y using Eq. (4). We further calculate the resonant angular frequency Ω using $\Delta\Omega/\Omega_0 = \Delta Y/2Y_0$. With the calculation of the resonant angular frequency shift $\Delta\Omega$ from dynamic strain, we update the strain amplitude R_A for the next cycle of the strain oscillation; we update R_A whenever the phase $\omega(t - t_1) = 0$ (link 3 in Fig. 1).

(3) We average $N_o(t)$ over the last cycle of the strain oscillation (with time duration $1/f_d$) during the sweep interval time Δt; from this averaged value, we calculate the resonant angular frequency Ω using the method mentioned in step 2.

(4) At time $t = t_1 + \Delta t$, we increase/decrease the driving frequency f_d by Δf. We calculate the oscillation strain amplitude $R_A(t_1 + \Delta t)$ using Eq. (8) for the driving frequency $f_d \pm \Delta f$ at $t = t_1 + \Delta t$; the recorded quantity for the response is the acceleration amplitude $\omega^2 R_A L_0$.

(5) We repeat steps 1, 2, 3, and 4 for each sampled driving frequency in the sweep and record the corresponding response. Figure 11 shows the time line of recursive steps 1, 2, 3, and 4 in the frequency sweep.

For a known dynamic strain, we solve Eq. (2) using the transition times τ_o and τ_c from Eq. (1) with energies E_o and E_c from the relationship in Fig. 3. We integrate the solution of Eq. (2) over barrier energy and obtain the softening ΔY from Eq. (4). The softening updates the response amplitude using Eq. (8) and the above-mentioned protocol.

APPENDIX B: STEADY-STATE SOLUTION

We can solve the equations listed for our model without considering the temporal evolution of the damage state N_o.

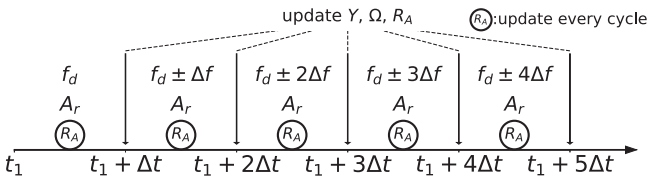

FIG. 11. Time line of the measurement protocol.

Instead, we solve for the stable equilibrium value of N_o from the following set of equations:

$$|R_A| = \frac{|A_r|}{\sqrt{(\omega^2 - \Omega^2)^2 + 4\gamma^2\omega^2}} \tag{B1}$$

and

$$N_o = \frac{1}{1 + \exp[(E_o - E_c)/k_B T]}. \tag{B2}$$

Equation (B1) is same as Eq. (8), and Eq. (B2) follows from the stable equilibrium solution in Eq. (3). The equilibrium fraction of open fractures n_{eq} is independent of the barrier energy, and hence N_o is equal to n_{eq}. The relations among other parameters are

$$E_o = B_0 - \frac{A_1}{1 + \exp[-(|R_A| - \mu)/\sigma]} \tag{B3}$$

and

$$E_c = A_0 + \frac{A_1}{1 + \exp[-(|R_A| - \mu)/\sigma]}, \tag{B4}$$

where the same sigmoid functions for the fracture energies are used (see Table I for used values of A_0, A_1, B_0, μ, and σ), and

$$Y = Y_0 - C_0(N_o - N_{\text{ori}}) \tag{B5}$$

and

$$\Omega = \pi\sqrt{Y/\rho}/L_0, \tag{B6}$$

where the feedback from damage N_o to the resonant frequency is taken into account. Equation (B5) is the same as Eq. (4), and Eq. (B6) is the equation used to convert Young's modulus Y into the resonant frequency.

Since $|R_A|$ influences E_o and E_c through Eqs. (B3) and (B4), and N_o feeds back to Ω through Eqs. (B5) and (B6), one can jointly solve Eqs. (B1) and (B2) together using an iterative adaption method [43], given the driving amplitude A_r and driving angular frequency $\omega = 2\pi f_d$. With an initial damage N_{oi}, one can solve for the stable equilibrium damage N_o. Since there is no dynamics in this approach, the solution corresponds to a stable equilibrium solution to which the nonlinear model will converge. There may be unstable equilibrium solutions, but the lack of stability precludes these solutions to be reached in the iterative process.

[1] J. A. TenCate and T. J. Shankland, Geophys. Res. Lett. **23**, 3019 (1996).

[2] J. A. TenCate, E. Smith, and R. A. Guyer, Phys. Rev. Lett. **85**, 1020 (2000).

[3] J. A. TenCate, Pure Appl. Geophys. **168**, 2211 (2011).
[4] K. Graff, *Wave Motion in Elastic Solids* (Dover Publications, New York, 1975).
[5] A. I. Korobov, N. I. Odina, and D. M. Mekhedov, Acoust. Phys. **59**, 387 (2013).
[6] J. Rivière, P. Shokouhi, R. A. Guyer, and P. A. Johnson, J. Geophys. Res.: Solid Earth **120**, 1587 (2015).
[7] P. A. Johnson, B. Zinszner, and P. N. J. Rasolofosaon, J. Geophys. Res.: Solid Earth **101**, 11553 (1996).
[8] M. Muller, A. Sutin, R. Guyer, M. Talmant, P. Laugier, and P. A. Johnson, J. Acoust. Soc. Am. **118**, 3946 (2005).
[9] R. Guyer and P. Johnson, *Nonlinear Mesoscopic Elasticity: The Complex Behaviour of Rocks, Soil, Concrete* (Wiley, New York, 2009), pp. 70–76.
[10] D. Pasqualini, K. Heitmann, J. A. TenCate, S. Habib, D. Higdon, and P. A. Johnson, J. Geophys. Res. Solid Earth **112**, 1 (2007).
[11] P. P. Delsanto, T. Whitcombe, H. H. Chaskelis, and R. B. Mignogna, Wave Motion **16**, 65 (1992).
[12] J. A. TenCate, D. Pasqualini, S. Habib, K. Heitmann, D. Higdon, and P. A. Johnson, Phys. Rev. Lett. **93**, 065501 (2004).
[13] R. A. Guyer, K. R. McCall, and K. Van Den Abeele, Geophys. Res. Lett. **25**, 1585 (1998).
[14] O. O. Vakhnenko, V. O. Vakhnenko, and T. J. Shankland, Phys. Rev. B **71**, 174103 (2005).
[15] V. Y. Zaitsev, V. E. Gusev, V. Tournat, and P. Richard, Phys. Rev. Lett. **112**, 108302 (2014).
[16] V. Gusev and V. Tournat, Phys. Rev. B **72**, 054104 (2005).
[17] V. Lyakhovsky, Y. Hamiel, J.-P. Ampuero, and Y. Ben-Zion, Geophys. J. Int. **178**, 910 (2009).
[18] L. Lemrich, P. A. Johnson, R. Guyer, X. Jia, and J. Carmeliet, Phys. Rev. E **96**, 062901 (2017).
[19] T. Brunet, X. Jia, and P. A. Johnson, Geophys. Res. Lett. **35**, L19308 (2008).
[20] Y. Komatsu and H. Tanaka, Phys. Rev. X **5**, 031025 (2015).
[21] A. V. Lebedev and L. A. Ostrovsky, Acoust. Phys. **60**, 555 (2014).
[22] Q. Li, T. E. Tullis, D. Goldsby, and R. W. Carpick, Nature (London) **480**, 233 (2011).
[23] R. Snieder and A. v. d. Beukel, Granular Matter **6**, 1 (2004).
[24] V. Zaitsev, V. Gusev, and B. Castagnede, Phys. Rev. Lett. **90**, 075501 (2003).
[25] M. R. J. Gibbs, J. E. Evetts, and J. A. Leake, J. Mater. Sci. **18**, 278 (1983).
[26] A. Amir, Y. Oreg, and Y. Imry, Proc. Nat. Acad. Sci. USA **109**, 1850 (2012).
[27] J. B. Walsh, J. Geophys. Res. **70**, 399 (1965).
[28] D. A. Lockner, J. B. Walsh, and J. D. Byerlee, J. Geophys. Res. **82**, 5374 (1977).
[29] K. C. E. Haller and C. M. Hedberg, Acoust. Phys. **58**, 713 (2012).
[30] P. A. Johnson, B. Zinszner, P. Rasolofosaon, F. Cohen-Tenoudji, and K. Van Den Abeele, J. Geophys. Res.: Solid Earth **109**, B02202 (2004).
[31] L. D. Landau, E. M. Lifshitz, A. M. Kosevich, and L. P. Pitaevskĭ, *Theory of Elasticity*, Course of Theoretical Physics (Elsevier, New York, 1986).
[32] D. J. Holcomb, J. Geophys. Res. Solid Earth **86**, 6235 (1981).
[33] J. Rivière, L. Pimienta, M. Scuderi, T. Candela, P. Shokouhi, J. Fortin, A. Schubnel, C. Marone, and P. A. Johnson, Geophys. Res. Lett. **43**, 3226 (2016).
[34] C. Sens-Schönfelder, R. Snieder, and X. Li (unpublished).
[35] R. Snieder, C. Sens-Schönfelder, and R. Wu, Geophys. J. Int. **208**, 1 (2017).
[36] P. Holmes and D. Rand, J. Sound Vibration **44**, 237 (1976).
[37] M. Brennan, I. Kovacic, A. Carrella, and T. Waters, J. Sound Vibration **318**, 1250 (2008).
[38] K. Magnus, *Vibrations* (Blackie & Son, Glasgow, Scotland, 1965).
[39] P. P. Delsanto and M. Scalerandi, Phys. Rev. B **68**, 064107 (2003).
[40] T.-P. Chang, Math. Probl. Eng. **2017**, 3769870 (2017).
[41] J. R. Rice, N. Lapusta, and K. Ranjith, J. Mech. Phys. Solids **49**, 1865 (2001).
[42] V. Lyakhovsky and Y. Ben-Zion, Geophys. J. Int. **172**, 651 (2008).
[43] A. H. Sherman, SIAM J. Numer. Anal. **15**, 755 (1978).